JOURNAL OF AIRCRAFT
Vol. 48, No. 4, July–August 2011

# Design of a Supersonic Natural Laminar Flow Wing–Body

E. Iuliano,* D. Quagliarella,† and R. S. Donelli‡
*Italian Aerospace Research Center, 81041 Capua, Italy*
I. Salah El Din§
*ONERA, 92190 Paris, France*
and
D. Arnal¶
*ONERA, 31055 Toulouse, France*

DOI: 10.2514/1.C031039

**The present investigation has been carried out within the SUPERTRAC project funded by the European Community in the 6th Framework Programme and aimed at investigating various techniques within laminar flow technology applied to supersonic drag reduction. In particular, this work deals with natural laminar flow shape design of a supersonic high-sweep wing–body configuration. The reference geometry has been provided by Dassault Aviation, one of the two industrial partners together with Airbus. Two different design are presented, produced by the Italian Aerospace Research Center and ONERA, respectively, using numerical optimization procedures based on evolutionary computing techniques and robust aerodynamic analysis tools. Results show how shape optimization can be effective in changing the boundary-layer characteristics of a supersonic high-swept wing and enhancing natural laminar flow on the wing surface.**

## Nomenclature

$A$ = wave amplitude function
$C_D$ = wing drag coefficient
$C_L$ = wing lift coefficient
$C_M$ = wing pitching moment coefficient
$C_p$ = pressure coefficient
$c$ = airfoil chord
$f_i$ = shape-modification functions
lam = laminar
ler = leading-edge radius
$M$ = Mach number
$N$ = amplification factor
$\bar{R}$ = attachment-line Reynolds number, $W_e/\sqrt{\nu\tilde{U}_e}$
$Re_x$ = Reynolds number based on $x$ abscissa
$\bar{R}^*$ = compressible attachment-line Reynolds number, $W_e/\sqrt{\nu^*\tilde{U}_e}$
sep = separation
$T$ = temperature
$T_e$ = boundary-layer edge temperature
$T_r$ = recovery temperature
$T_w$ = surface wall temperature
$T^*$ = reference temperature, $T_e + 0.1(T_w - T_e) + 0.6(T_r - T_e)$
$t$ = time
tea = trailing-edge angle
tr = transition
$U_e$ = chordwise velocity component
$\tilde{U}_e$ = chordwise velocity gradient at stagnation, $\mathrm{d}U_e/\mathrm{d}x$
$W_e$ = spanwise velocity component
$w_i$ = shape-modification function weights (design variables)
$x$ = abscissa along the airfoil chord
$y$ = abscissa along the wingspan
$z$ = abscissa normal to airfoil chord
$\bar{x}$ = abscissa normal to leading edge
$\bar{y}$ = abscissa normal to wall
$\bar{z}$ = abscissa parallel to leading edge
$\alpha$ = wave number along $\bar{x}$
$\beta$ = wave number along $\bar{z}$
$\Lambda$ = sweep angle
$\nu$ = air kinematic viscosity
$\nu^*$ = air kinematic viscosity evaluated at $T^*$
$\sigma$ = imaginary part of the disturbance growth rate
$\omega$ = wave frequency

## I. Introduction

THE supersonic civil transport aircraft is still a challenge for the aeronautical scientific community. At supersonic speeds, the high amount of drag and noise levels requires a careful design process that is capable of providing innovative aircraft configurations and aerodynamic shapes. Since the Concorde and Tu-144 aircraft, several design ideas have been proposed, but none of them have been put into practice. This has been mainly due to the loss in aerodynamic efficiency and the economic implications that are embedded in the supersonic flight. In recent years, many government/industrial-funded projects have been devoted to find new engineering solutions to these well-known problems. In this context, one of the main objectives of the last 10 years has been to maximize the laminar flow portion on supersonic wings. As friction drag can account for about 20–40% of the total drag at supersonic speeds, a delay of the laminar-to-turbulent transition could allow large weight and fuel savings. It is well known that boundary-layer transition on swept wings is caused by small perturbations that grow as they propagate downstream. A standard method to predict transition, often used in industrial applications, is the $e^N$ method [1]. The $e^N$ method has been applied in this design process, since it has already been used in the supersonic regime [2,3].

Presented as Paper 2009-1279 at the 47th AIAA Aerospace Sciences Meeting, Orlando, FL, 5–8 January 2009; received 25 March 2010; revision received 8 November 2010; accepted for publication 9 November 2010. 

*Aerospace Research Engineer, Applied Aerodynamics and Aeroacoustics Laboratory, Via Maiorise; e.iuliano@cira.it.
†Aerospace Research Engineer, Applied Aerodynamics and Aeroacoustics Laboratory, Via Maiorise; d.quagliarella@cira.it.
‡Aerospace Research Engineer, Aerodynamics and Aeroacoustics Methods Laboratory, Via Maiorise; r.donelli@cira.it.
§Aeronautical Research Engineer, Applied Aerodynamics Department, 8 Rue des Vertugadins; itham.Salah_el_din@onera.fr.
¶Aeronautical Research Engineer, Aerodynamics and Energetics Modeling Department, 2 Avenue Edouard Belin; Daniel.Arnal@onecert.fr.

A design task aiming only at delaying transition could be ineffective, or even negative, when looking at global wing performance; other features should also be addressed as key elements, such as pressure drag reduction, noise reduction, structural design, fuel volume, and subsonic performance. For instance, the leading-edge sweep angle should be carefully evaluated, because it has a strong effect on low-speed aerodynamics, drag characteristics, and structural design. Indeed, the possibility of maintaining extensive laminar flow over a low-sweep wing is confirmed by experimental data [4–6] and theory [7,8]. However, as the wing would have high inviscid drag, the corresponding airfoil section should be designed to be thin with a sharp leading edge. As a consequence, the structural stiffness and the subsonic stall behavior would be negatively affected. On the other hand, a high-sweep wing design with subsonic leading edge does not present these negative features, but obtaining large regions of laminar flow is a very difficult challenge, due to high Reynolds numbers, adverse pressure gradients, and highly-three-dimensional flow structures. In other words, a supersonic wing design requires a multidisciplinary and multipoint approach. Recently, the NEXST project by the Japan Aerospace Exploration Agency [9,10] proved the possibility to achieve extended natural laminar flow both numerically and experimentally, even for highly swept wings. In their work, the wing airfoil shapes and twist distribution were designed using an inverse method and boundary-layer stability analysis tools [3,11]. The numerical and experimental campaigns were performed on a subscaled airplane model and hence at a very low Reynolds number (about 11% of the full-scale concept).

The present work is mainly focused on the aerodynamic shape optimization of a high-sweep wing for a supersonic business-jet configuration in order to achieve natural laminar flow (NLF). A fully 3-D transition prediction procedure is presented here as the core analysis tool in an optimization framework based on evolutionary algorithms. Indeed, current computational fluid dynamics (CFD) solvers, mostly based on Reynolds-averaged Navier–Stokes (RANS) equations, and viscous–inviscid interaction tools are not able to predict the onset of transition, because they lack the information about the growth of boundary-layer disturbances. Hence, in order to accurately predict the transition location, three chained computations are generally required: an aerodynamic flow solution to obtain the external mean flow, a boundary-layer computation, and a stability analysis of boundary-layer velocity profiles.

Several tools may be used to perform such computations with different levels of fidelity in flow physics modeling. The design chain and tools used in the present research will be detailed in the following sections. The design task is carried out within the SUPERTRAC (Supersonic Transition Control) project, funded by the European Community within the 6th Framework Programme (2005–2008). The objective of the aerodynamic shape design is to numerically demonstrate that the laminar portion of the wing can be increased even in challenging design conditions by means of suitable parameterizations and accurate flow solvers. Two partners have been involved in the present work: namely, CIRA and ONERA; even though they share nearly the same tools for aerodynamic evaluation, the adopted optimization strategy and the wing geometry parameterizations are different. Both approaches and results are presented and discussed.

## II. SUPERTRAC Project Framework

The study of laminar–turbulent transition is of great importance in many fluid-dynamic applications, since the magnitude of viscosity and heat transfer increases considerably as the flow becomes turbulent. The accurate prediction of the transition location (for instance, on a wing surface) is then a prerequisite for accurately predicting the drag. In the last 20 years the interest in laminar flow technology has grown rapidly because of the large benefits envisaged in its application on modern aircraft, due to energy savings and environmental advantages [12]. For commercial transport aircraft, the achievement of laminarization would significantly reduce the drag of wings, tails, or nacelles with respect to conventional design, which is usually fully turbulent. The feasibility and potential benefits of laminarization for subsonic/transonic transport configurations have been evaluated and demonstrated in many wind-tunnel and flight experiments [13–15]. The problem has been and is still widely studied for subsonic and transonic flows, but little is known about the feasibility of laminar flow control techniques at supersonic speeds. The extension of the low-speed laminar flow techniques to supersonic configurations is not obvious and requires specific investigations. The objective of the SUPERTRAC project is to investigate the possibilities to apply the laminar flow technology to supersonic aircraft wings, such as micron-sized roughness, anticontamination devices, laminar flow control by suction, and natural laminar flow shape optimization. Indeed, future air traffic vision aims at severe requirements on emission and noise that are directly related to weight, size, fuel burn and drag reduction. The SUPERTRAC project, coordinated by ONERA, involved nine partners, including two European aircraft manufacturers. All the partners have already participated in previous European research projects devoted to laminar transonic aircraft development [16,17] (ELFIN, HYLDA, HYLTEC, EUROTRANS, and ALTTA).

## III. Transition Mechanisms: Theory Background

### A. Phenomenological Description

In this section the phenomena causing a laminar boundary layer to become turbulent on a swept wing are discussed. There are at least three main mechanisms that govern transition phenomena and that have to be considered [18] (see Fig. 1).

First, the attachment-line contamination that occurs when turbulence convected along the fuselage propagates along the swept leading edge and then contaminates the wing surface. This kind of instability is strongly affected by the leading-edge wing radius, as observed by Pfenninger [19] during the laminar flow control flight tests with the X21 aircraft. He formulated a criterion, later perfected by Poll [20,21], based on the attachment-line Reynolds number $\bar{R} < 245$. For compressible flows, a modified Reynolds number $\bar{R}^*$ is used [22]. The criterion attachment-line contamination to be avoided if an appropriate sweep and curvature of the leading edge are selected.

The other two mechanisms have a common origin. Close to the leading edge, in a region known as the *receptivity region*, according to Morkovin [23,24], the external disturbances, such as freestream turbulence, engine noise, acoustic waves, enter the boundary layer and generate unstable waves. This is obtained through the effect of the boundary layer growing in the neighborhood of the leading edge, wall roughness, wall waviness, and blowing/suction. The above-introduced receptivity mechanism can trigger the amplification of Tollmien–Schlichting (TS) and crossflow (CF) waves. TS waves are the result of the instability of the streamwise mean velocity profile, i.e., the component of the mean velocity profile in the external streamline direction. These waves are unstable in regions of zero or positive pressure gradients. Their evolution is fairly well described by the linear stability theory [25,26]. CF waves are the result of the

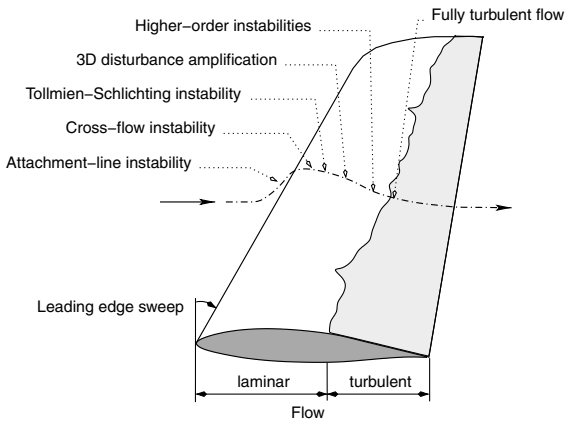


**Fig. 1 Transition phenomena on a swept wing.**

instability of the crossflow mean velocity profile. These waves are unstable in regions of negative pressure gradient, typically in the vicinity of the leading edge where the flow is strongly accelerated. When the wave amplitude becomes finite, nonlinear interactions occur and lead rapidly to turbulence.

### B. Transition-Delaying Strategy

Delaying the onset of transition requires to modify the mean velocity field and/or the instability mechanisms in such a way that the growth rate of TS and CF waves is reduced. This objective may be achieved by using three strategies:

1) Natural laminar flow control consists of optimizing the wing shape in order to maximize the laminar flow portion.

2) Laminar flow control modifies the boundary-layer velocity profile by applying a small amount of suction at the wall.

3) Hybrid laminar flow control combines the previous two approaches.

The present work deals with the natural laminar flow control strategy. To design a shape with extended laminar flow, the hypothesis of a linear evolution of the boundary-layer disturbances is sufficient. In this context, the most common transition prediction method is the $e^N$ method [1,2,27]. This method is based on the relative amplification of the discrete frequency disturbance, which first reaches a preset transition level of $e^N$. The $e^N$ method involves the stability analysis of the laminar boundary layer by solving the linear equations of the nonstationary disturbances superposed to the basic motion. Under the assumption of quasi-parallel flow, the linearized Navier–Stokes equations admit a normal mode solution in the form of a harmonic wave:

$$\varphi(\bar{x}, \bar{y}, \bar{z}, t) = A(\bar{y})e^{i(\alpha\bar{x}+\beta\bar{z}-\omega t)} \tag{1}$$

where $\varphi$ is a velocity, pressure, or density fluctuations. Introducing the previous expression in the linearized Navier–Stokes equations, a system of ordinary differential equations for compressible flow is obtained: these equations and the related boundary conditions are homogenous and represent an eigenvalue problem that admits a nontrivial solution only when the dispersion relation $\omega = \omega(\alpha, \beta)$ is satisfied [25]. Usually, the problem is solved by following two different theories: a spatial theory, where $\alpha$ and $\beta$ are assumed to be complex and $\omega$ real, and a temporal theory, where $\alpha$ and $\beta$ are assumed to be real and $\omega$ complex.

The solution of the linear system of equations allows the growth rate of the disturbances to be determined. The $N$ factor represents the amplitude ratio for each frequency obtained by integrating the spatial amplification rate as follows:

$$N = \log\left(\frac{A}{A_0}\right) = \int_{x_0}^{x} -\sigma(x)\,\mathrm{d}x \tag{2}$$

where $\sigma$ is the imaginary part of the disturbance growth rate, and $A_0$ is the wave amplitude at $x = x_0$.

## IV. Design Target

The objective of the present work is the design of a supersonic wing with enhanced natural laminar flow characteristics, as well as the understanding of the aerodynamic and geometric features that can drive the optimization toward NLF enhancement. Indeed, such a kind of optimization has not been attempted in previous works; therefore, a solid expertise and scientific background on the results cannot be obtained. This makes it of paramount importance to give a physical interpretation to the results coming from the optimization process.

The reference configuration is the wing–body shape optimized within the framework of Supersonic Business Jet project of Dassault Aviation and made available within SUPERTRAC project. A sketch of the geometry is given in Fig. 2. The inboard wing has a 65° leading-edge sweep angle, and the outboard-wing sweep is 56°. The wing semispan is 9.35 m and the aspect ratio is 3.5. The cruise flight Mach number is 1.6. Previous investigations [28] showed that the


**Fig. 2 Baseline geometry.**

baseline airfoil presented a very short extent of laminar flow, and transition was triggered by both CF and TS waves. A redesign of the wing airfoil at a selected station was agreed upon among the SUPERTRAC partners in order to build a new reference shape for the wing design phase, which is described here. The target is to optimize the wing section airfoils and twist angle in order to maximize the laminar flow region while monitoring and controlling the pressure (vortex and wave) drag.

To this aim, given the aerodynamic design problem, a numerical optimization procedure is used. Generally speaking, the problem of searching a solution to a minimization problem strongly depends on the shape of the objective functions and on the set of constraints. As neither the objective function nor the imposed constraints can be a priori cast in closed form, the exploration of the design space can get very computationally intensive, especially if the target function has a highly multimodal profile. Indeed, the presence of several local minima can trap a gradient-based algorithm in a suboptimal solution or negatively impact the convergence of an evolutionary-based algorithm, even if the naturally explorative characteristics of the latter have shown to be potentially able to approximate the true optimum or the set of optima. Moreover, the specific problem under analysis usually requires a proper parameterization and many design variables to control not only the profile shape, but also its distribution along the spanwise direction, possibly the twist angle and the thickness ratio distribution. Therefore, the designer has to deal with the multimodal and high-dimensional character of the objective function, which greatly increases the complexity of the search approach. The problem gets even more complicated considering the partial lack of literature in the peculiar field of supersonic laminar flow wing design, which does not provide sufficient guidelines toward the optimal solution. Hence, a proper, highly explorative, design strategy must be defined and assessed. The two partners, CIRA and ONERA, have split the design space exploration into two different optimization strategies, named *global* and *local*. It must be emphasized once again that the two approaches do not refer to the search method in itself, but to the investigation of the relationship between physical parameters and design variables, i.e., the adopted parameterization. Indeed, the global search aims at finding the optimal solution by modifying the wing profiles shape along the full chord and span. The advantage of this approach is to let the whole shape vary according to the variation of the aerodynamic conditions along the wing, e.g., local Mach number, Reynolds number, and downwash. This feature allows more flexibility especially in satisfying aerodynamic constraints on total lift, drag, and pitching moment coefficients while optimizing for natural laminar flow. On the other hand, the local approach is focused on local shape modification around the wing leading edge, a region in which it is more likely, according to previous design experience, that a shape change can introduce a different flow behavior in terms of laminarity. The local search aims at analyzing in detail the sensitivity of natural laminar flow improvement to local shape change, where this sensitivity is as high as possible. In other words, this is like a trust-region approach, where the region to trust is not sought iteratively, but is supposed to be already known from past knowledge. Even though sharing a similar evolutionary-based optimization method, the two approaches are supplementary, because they look at the

design space from two different perspectives (global and local) while aiming at the same goal. In principle, this choice is made possible just by the peculiar problem under study: indeed, previous works [3,11] already showed that the design of a supersonic swept wing for natural laminar flow under aerodynamic and geometrical constraints has to properly and carefully balance leading-edge design, overall wing profile shape and twist distribution. As reported in later sections, this design hints are also the core experience and knowledge drawn by the authors during the presented design research.

## V. Design Methodology

Before getting into the specification of the problem formulations, the design methodology adopted by both approaches, which are quite close in the principle, is given. The method used to perform the wing design is based on numerical optimization. The whole process can be split into two main components, the optimizer, controlling the scan of the design space and the analyzer, evaluating the performance of a configuration on the optimizer request. A stochastic evolutionary-based approach has been chosen to solve this problem considering the numerous tools involved in the evaluation of the performance process of a single aircraft design and the design space wideness. Apart from accuracy considerations, the main drawback of a classical gradient approach (via finite differences) is the numerous computations needed for one optimizer iteration considering the great number of design variables involved in the parameterization. More up-to-date approaches for gradient computations such as adjoint state resolution [29] would allow this problem to be overcome. Unfortunately, even though effective for the CFD solver, such techniques must still be made compatible with the three-dimensional transition prediction tools. Objective and constraint functions have been defined in order to ensure the geometrical and aerodynamic fitness to the requirements. The fitness is evaluated through an automatic procedure that performs sequentially a 3-D Euler aerodynamic analysis, a 3-D boundary-layer computation and a boundary-layer stability analysis. Hence, global aerodynamic coefficients, boundary-layer parameters and laminar-to-turbulent transition predictions are simultaneously available to build up the cost function to minimize.

## VI. Design Chains and Tools

### A. Chains Overview

This section is dedicated to the detailed description of the various stages and tools of the two optimization processes that are sketched in Fig. 3. Basically, the loop is made up of an optimizer, a configuration/mesh generator and an evaluation module, each exchanging data and information with only one of each other: the optimizer and the configuration generator communicate through design variables; the configuration geometry is submitted to the evaluation module, which returns the values of constraints and objectives to the optimizer.

The fitness function can take into account several components of the aerodynamic performance, such as inviscid drag, transition and laminar separation location, and lift and pitching moment coefficients. These terms can be computed for one or more design points and can be freely combined into one or more objective functions and constraints. Furthermore, each performance term can be either directly summed (through a weight) into a given objective or constraint either filtered through some predefined penalty functions. Constraints may also be of geometrical nature, such as maximum thickness or wing box layout and volume. Some constraints, like lift force, may also be directly satisfied through the variation of a free parameter, such as the incidence angle.

### B. Optimization Algorithms and Process Management

Genetic algorithms (GAs) are based on evolutionary concepts implying operators such as several types of mutation and crossover operators. Even though both approaches use a GA, they do not share the same tools. The global approach calls an in-house CIRA evolutionary optimization tool, GAW [30–33], which can handle, in addition to the GA management, multipoint and multiobjective constrained problems and is also able to use hybrid operators

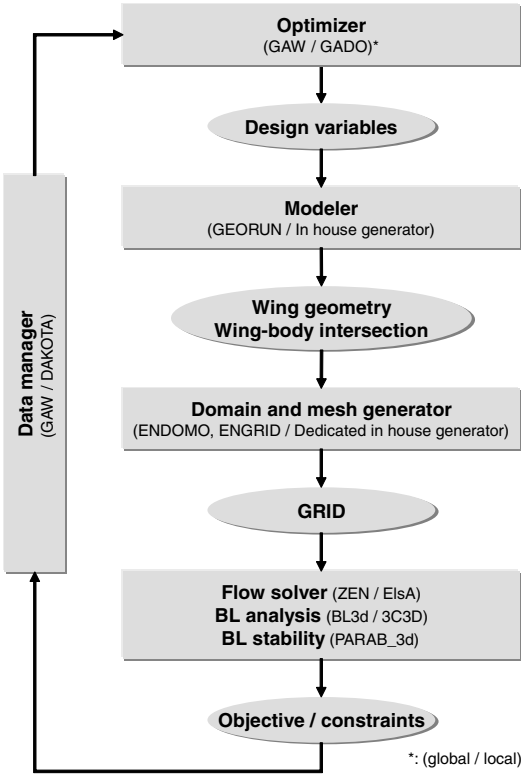


**Fig. 3 Wing design chain.**

adopting classical gradient-based algorithms. When facing a multiobjective problem, the GA can directly use the defined dominance criteria to select elements appointed to reproduction and to hence drive the evolution of the population toward the Pareto front. The selection operator used here is random walk. The locally nondominated population elements met in the walk are selected for reproduction. If more nondominated solutions are met, then the first one encountered is selected. At the end of every new generation, the set of Pareto optimal solutions is updated and stored. A kind of extension of the elitism strategy to multiobjective optimization is obtained by randomly selecting an assigned percentage of parents from the current set of nondominated solutions.

Concerning the second approach, called local, the GADO [34] library, based on a genetic algorithm and integrated in the DAKOTA [35] open source optimization suite was chosen. The flexibility of DAKOTA, which integrates various capabilities from the management of typical gradient-based approaches to complex surrogate models, has proven useful and efficient in previous studies [36].

### C. Parameterization and Automatic Configuration: Mesh Generation

The key feature of both design systems is the capability of performing the automatic remeshing of new configurations, for fixed topological connections and grid tuning parameters. The surfaces of new configurations are generated on the base of geometrical parameters, which are linked to some of the design variables controlled by the optimizer. When dealing with an optimization problem the parameterization refers to the link between the design variables and the global shape of the configuration under study: in an aeronautic frame like the present, the parameterization acts on the real geometry, which has to be modeled according to the modification of the design variables. Once chosen a reference configuration (here conventionally corresponding to the configuration obtained by setting all design variables to zero), links between geometric parameters and design variables are set in the problem definition phase and arranged in a database file. In principle, it would be possible to link each configuration modification to a design variable, but it can be useful to exploit general rules or functions to modify a set of parameters with one design variable. The capability of modifying the reference geometry in different ways, depending on the specific problem, can

improve the efficiency of the optimization process. As an example, the database format for aerodynamic shape of wings has been designed in such a way that parameters are familiar to the aerodynamicist. Taper ratio, sweep angle, twist angle, maximum thickness distribution along the wingspan are typical parameters. Each of these geometrical items can be activated and linked to a specific design variable. The airfoil shapes throughout the wing are controlled by using a list of points. They can be modified either by adding predefined shape functions to the reference geometry and by moving some control points through a bispline approach [37].

To generate the new mesh, specific set of input data are required in both cases: the topology of the domain (i.e., how blocks are connected to each other), the geometry (i.e., the shape of each block), the grid dimensions (how many cells have to be generated in each block) and the grid parameters (how the grid cells have to be sized and clustered). To generate a family of meshes that share the same characteristics during the design process, the topology data, grid sizes and parameters are kept fixed. This is useful within the automatic procedure and also for better comparisons of flow solutions. Indeed, drag computation is very sensitive to grid density, particularly when meshes are not very fine. The procedure helps to maintain a standard grid quality during the remeshing of new configurations in the optimization loop.

For the global approach, in-house software is used to build computational volume grids. The GEORUN [30] geometry generator, the ENDOMO [38] domain modeler, and the ENGRID [39,40] multiblock structured-grid generator have been chained to generate topologically similar grids on geometrically different aerodynamic shapes. For the second approach, the surface meshing was generated using ICEM HEXA mesh generator. Then an analytical deformation tool is coupled with an automated mesh generator dedicated to supersonic configurations to build the volume mesh.

### D. CFD Flow Solvers

The aerodynamic analysis system is based on a structured multiblock approach [41–44]. The in-house-developed ZEN (CIRA) and elsA (ONERA) flow solvers are multizonal Euler–RANS solvers, with several turbulence models implemented. Spatial discretization is performed by finite volume, central schemes, or decentral schemes, with second- and fourth-order artificial dissipation. Convergence toward steady solution is obtained using explicit Runge–Kutta formulas, with implicit residual smoothing and multigrid acceleration techniques. The flow solvers are fully vectorized. These features represent a compromise choice between efficiency and accuracy, since an optimization procedure requires the analysis of hundreds of configurations.

### E. Three-Dimensional Boundary-Layer and Stability Computation

To estimate the laminar-to-turbulent transition onto a wing surface, several methods can be used, but the designer usually aims at obtaining an acceptable compromise between accuracy and speed, because the number of computations to perform in a design process may be very high. The present approach consist of a 3-D Euler inviscid solution coupled to a fully-three-dimensional finite difference boundary-layer analysis. This choice allows the basic features of both the external aerodynamic flowfield (like shock waves, pressure gradient, and wing loading) and the laminar/turbulent boundary-layer flow (both streamwise and crossflow velocity profiles, temperature profiles, and integral quantities) to be caught. Once known the spatial evolution of the laminar boundary layer, a method based on the linear stability theory coupled to the $e^N$ method is applied to check for laminar-to-turbulent transition. A general view of the transition prediction cascade is given in Fig. 4.

#### *1. Three-Dimensional Boundary-Layer Computation Method*

The three-dimensional boundary-layer method is based on the finite difference scheme developed by Cebeci [45] for the global approach and on the 3C3D [46] solver for the local approach. Both codes are able to solve compressible laminar/turbulent flows on finite wings with and without suction through either the full three-dimensional or the quasi three-dimensional boundary-layer equations [47].

The solution of the three-dimensional equations, where streamwise velocity $u$ and spanwise velocity $w$ components are positive, can be achieved easily with the finite difference methods of

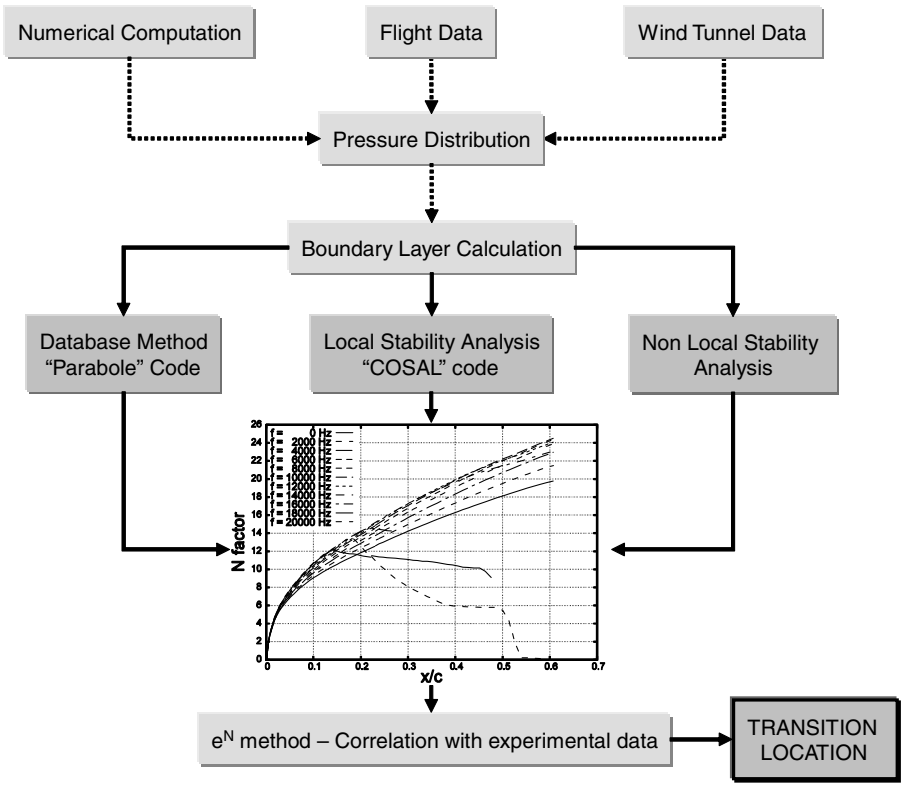


**Fig. 4 Flowchart of transition prediction on wings.**

Crank-Nicolson and Keller , as described in [48]. When the spanwise velocity component contains regions of flow reversal, however, the solution of three-dimensional boundary-layer equations is not so straightforward and requires special procedures to avoid the numerical instabilties that can result from reversal in $w$. For simplicity and robustness, the zigzag box scheme [48] is used in this case.

The boundary-layer method is formulated in the standard mode, i.e., it requires that the external velocity distribution is given in addition to the freestream conditions and wing geometry. It assumes that there is no flow separation on the wing; if one is found, then the calculations are terminated at the location where the chordwise wall shear force vanishes.

### 2. *Boundary-Layer Stability Analysis*

Many industrial tools based on the local linear stability theory, coupled with $e^N$ method have been developed in these years. These tools are very fast, but the huge quantity of calculations necessary to predict the transition location is often time consuming. Furthermore, most of these methods require a convergence procedure, which cannot be easily executed automatically. For these reasons ONERA-CERT developed the so-called database method [49,50]. This method is based on the idea to analytically represent the growth rate of unstable disturbances as a function of some relevant boundary-layer parameters [51–53]. The database method is able to compute the growth rates of Tollmien–Schlichting and crossflow waves. The main notations are given in Fig. 5. At a given point on the wing, $\theta$ is the local angle between the external streamline and the $x$ axis and $\psi$ is the angle between a chosen direction and the external streamline. The coordinate system is referenced as $(x, z, y)$, where $y$ is the normal to the wall. The basic flow, resulting from a laminar boundary-layer computation, provides the local velocity profiles $\bar{U}(y)$ and $\bar{W}(y)$. These profiles are projected in a given direction (corresponding to the wave angle direction $\psi$) leading to a 2-D projected velocity profile $\bar{U}_{2D}(y)$. The latter is inflexional for a projection angle $\psi$ sufficiently large. The main idea of the database is to guess that the growth rate may be approximated with only a prescribed frequency, the projected Reynolds number $R_{2D}$ (i.e., calculated with the external projected velocity $\bar{U}_{e,2D}$, and the displacement thickness $\delta_{1,2D}$ calculated with the projected velocity profile $\bar{U}_{2D}(y)$) and two parameters:

$$U_i = \bar{U}_{2D}(y_i) \qquad P = y_i \left( \frac{\mathrm{d}U_{2D}}{\mathrm{d}y} \right)_{y=y_i}$$

where $y_i$ is the distance of the inflexion point from the wall. It is implicitly assumed that all the quantities in the previous expressions are dimensionless according to $\bar{U}_{e,2D}$ and $\delta_{1,2D}$. Then for a given value of these two key parameters $(U_i, P)$, that means for a given physical mean boundary-layer abscissa $(\bar{U}(y), \bar{W}(y))$, it is guessed that for a given frequency, the growth rate $\sigma_{2D}$ of the projected profile has a universal dependence with respect to the Reynolds number $R_{2D}$ in the form of two half-parabolas (see Fig. 5). These two half-parabolas may be characterized by $R_0$, $R_m$, $R_1$, and $\sigma_m$ for, respectively, the critical Reynolds number, the Reynolds number corresponding to the maximum of amplification, the second critical Reynolds number (branch II of the neutral curve), and the value of the maximum of amplification. All of these quantities refer to the projected mean velocity profile. These four coefficients are simple analytical functions of the frequency with coefficients that only depend on $U_i$ and $P$. It has been proven that the final expressions obtained work rather efficiently, with a maximum of 10% of difference in comparison with exact stability results (and with a ratio of computation effort in the range of $10^5$ !). The above expressions do not work for the zero frequency, but the approach has been extended by ONERA in cooperation with CIRA [51]. In fact, the two parameters have been computed with the assumption that, for practical cases, the projected Reynolds number and the corresponding growth rate are more or less limited in a region close to $R_0$ (as given in Fig. 5). A new simple analytical relationship between the growth rate and the projected Reynolds number for given values of $U_i$ and $P$ has been found [54]. Figure 5 shows the comparison of the estimated and exact spatial amplification rate, when the asymptotic value of the projected growth rate $\sigma_\infty$ is approximated with an analytical relationship.

### 3. *Choice of Critical N Factor*

It is well known to the aeronautical scientific community that the use of the $e^N$ method is subject to the choice of the critical $N$ factor at transition. Several investigations have been performed to find calibrations and exploit correlations able to accurately predict transition through $e^N$ method in transonic flows [13–17]. However, to the authors' knowledge, no similar data are available for supersonic flows. Hence, as the main objective of the present research is to investigate the potential to enhance the laminar flow on a supersonic leading-edge wing through shape optimization rather than to design a new wing, the $N$ factor at transition is expected and assumed to be a plausible and approximate (but tested) value, rather than a precise threshold. As a consequence, the expertise and knowledge acquired in past successful research projects have been exploited to this aim. In

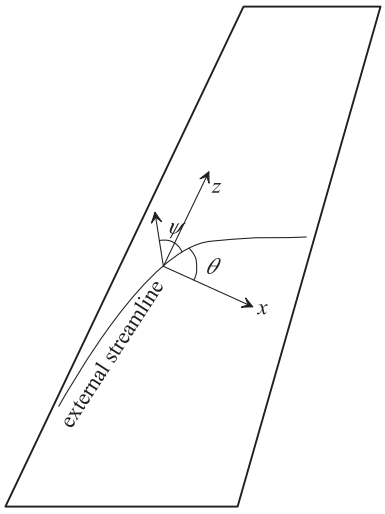


**a) Coordinate system**

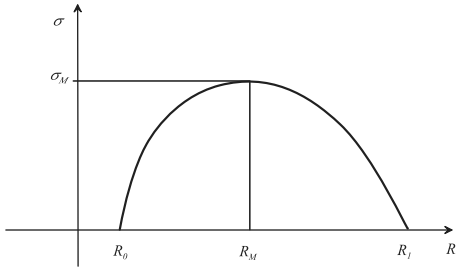


**b) Two half parabolas express the Reynolds dependance of the local growth rate, for the nonzero frequencies**

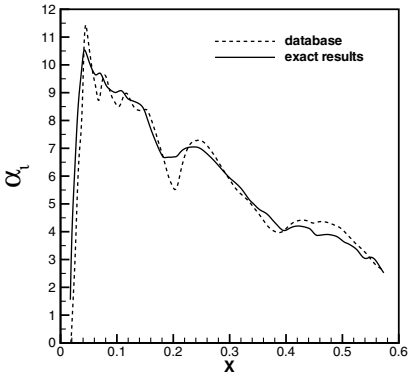


**c) Comparison of the exact and the estimated growth rate $\sigma_{3D}$ for fixed dimensional spanwise wave numbers $\beta$ = 1000 m$^{-1}$**

**Fig. 5 Database method.**

particular, during the ELFIN II European project, numerical computations using the database envelope method were compared with Fokker 100 flight-test data; one of the conclusions of such an investigation was that [55],

> The scatter of *N* factors is quite reasonable, despite whether the flow has been treated as compressible or incompressible, with or without the presence of curvature effects. The calibrated *N* factors, in most cases, are in the range of 15 or above for compressible without curvature....Compressibility has a moderate effect on stabilising the disturbances.

Since compressibility has a damping, and hence stabilizing, effect on boundary-layer disturbances, a transition $N$ factor of 15 is assumed to be a suitable value for supersonic cases and is used here to detect the transition location on a supersonic wing throughout the design process.

## VII. Parameterization and Optimization Problem Formulations

The problem definition phase includes the identification of design variables, objectives and constraints to be handled in the optimization process. As mentioned above, CIRA and ONERA applied two different approaches in the problem definition phase, while sharing the same design conditions and constraints. The global approach (CIRA) consisted of investigating a wide design space made of about 200 variables to allow for a wide range of possible shape modifications, along both the wing chord and the wingspan. After a preliminary sensitivity analysis, the local approach (ONERA) consisted of performing local airfoil shape modifications applied in the vicinity of the leading edge, combined with global spanwise geometrical deformations.

### A. Global Approach (CIRA)

#### 1. *Parameterization*

The global search approach followed by CIRA aims at investigating and successively defining the wing shape characteristics that could promote the laminar flow in supersonic conditions. Much is known [12], even in the supersonic regime [3], about how the airfoil pressure distributions should be to reach wide regions of laminarity, but it is not straightforward to find the corresponding shape, which also depends on the flow conditions, wing planform, and actual design constraints. Moreover, it is expected that the fuselage presence effects and the varying aerodynamic conditions along the wingspan (e.g., the Reynolds number varies from about $80 \times 10^6$ at the wing root to $16 \times 10^6$ at the wing tip) would radically modify the resulting shape of the wing in the spanwise direction. Hence, a proper parameterization is introduced either to catch this feature and to ensure the geometry smoothness throughout the wingspan. Wing section shape modification is carried out by following the modification functions approach: 68 predefined functions, acting both on airfoil mean line and thickness distribution, are added to the baseline shape by using weight coefficients through the following formula:

$$z(x) = z_0(x) + \sum_{i=1}^{n} w_i f_i(x)$$

where $z(x)$ is the modified shape and $z_0(x)$ is the baseline shape. Using this approach, the shape design variables are represented by the weights of the modification functions and the corresponding ranges are chosen following designer experience or a trial and error process. The $f_i$ are chosen among the classical airfoil design modification functions, like the Hicks–Henne, Wagner, and Legendre functions [37], but they include also wave, sinusoidal, and rear loading functions to locally modify the airfoil shape. To correlate the shape modifications along the wingspan, design variables involving section geometry modifications (shape and twist angle) are recombined into new design variables by using a linear transformation matrix. This allows the uniformity and regularity of shape-modification distribution throughout the wing and the reduction of the total number of design variables handled by the optimizer. The general law for design-variable transformation is given by the following matrix form:

$$\begin{bmatrix} v_1 \\ v_2 \\ \vdots \\ v_m \end{bmatrix} = \begin{bmatrix} W_{11} & W_{12} & \cdots & W_{1p} \\ W_{21} & W_{22} & \cdots & W_{2p} \\ \vdots & \vdots & \vdots & \vdots \\ W_{m1} & W_{m2} & \cdots & W_{mp} \end{bmatrix} \begin{bmatrix} V_1 \\ V_2 \\ \vdots \\ V_p \end{bmatrix}$$

where $V_i\ (i = 1, \ldots, p)$ are the old design variables, $v_i\ (i = 1, \ldots, m)$ are the new design variables, and $W_{ik}$ $(i = 1, \ldots, m$ and $k = 1, \ldots, p)$ are the transformation weights, with $m < p$. Among the various functionalities that this approach allows, for instance, is to obtain any twist angle distribution law (e.g., linear, quadratic, and piecewise linear) along the span length or to connect the shape modification between different portions of the wing. Twenty-five wing sections have been selected for parameterization and wing geometry definition, but only three of them (namely, the root, kink, and tip sections) are effectively involved and controlled in the global shape modification. Indeed, the adoption of the transformation matrix allows the spread of each design variable throughout the wingspan, e.g., by using piecewise linear functions, as shown schematically in Fig. 6. The left-hand figure depicts the piecewise weight functions for shape and twist design variables versus the span length. For instance, the modification of the inboard section shape (dotted line, labeled as inboard-wing shape) does not have any effect on the outboard wing, because in that region the weight of each

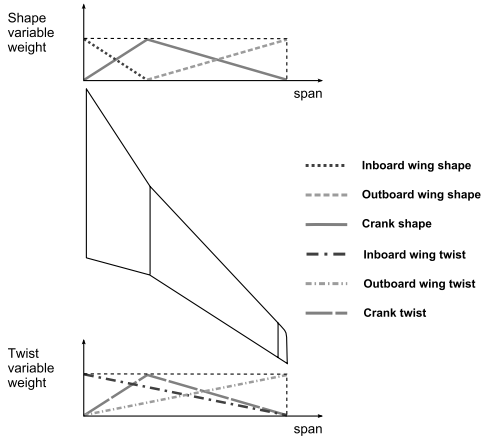


**a) Global approach - design variables spread along the wing span**

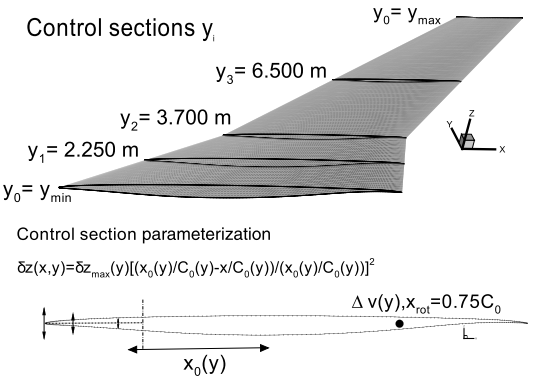


**b) Local approach**

**Fig. 6 Parameterization details.**

root-section shape design variable is zero. The total number of design variables is 208, resulting from 68 airfoil shape variables for each control wing section (204 total variables), three variables to control the twist angle, and one additional variable to modify the wing-fuselage setting angle.

*2. Optimization Problem*

A synoptic view of design condition, constraints and objective as set up by CIRA is given in Table 1. The objective function $\boldsymbol{G}(C_D, C_L, C_M, \text{ler}, \text{tea}, \Delta x_{\text{lam}})$ includes some penalty functions to take into account for constraints, and it is defined as

$$\boldsymbol{G} = kP(C_D - \tilde{C}_D) + nP(\tilde{C}_L - C_L) + mP(\tilde{C}_M - C_M) + qP(\Delta x_{\text{lam}}) + \ell P(\tilde{\text{ler}} - \text{ler}) + tP(\tilde{\text{tea}} - \text{tea})$$

where $k$, $n$, $m$, $q$, $\ell$, and $t$ are constant values that define the relative importance of the corresponding aerodynamic/geometric performance component. The quadratic penalty function is activated in a quadratic mode only if its argument is positive. Hence, $P$ has the following expression:

$$P(x) = \begin{cases} x^2 & \text{if } x > 0 \\ 0 & \text{if } x \le 0 \end{cases}$$

The function $\Delta x_{\text{lam}}$ is introduced to estimate the transition and laminar separation position on the whole wing, and it is defined as

$$\Delta x_{\text{lam}} = \sum_{i=1}^{n} (\Delta x_{\text{lu}} + \Delta x_{\text{ll}} + \Delta x_{\text{su}} + \Delta x_{\text{sl}})$$

where

$$\Delta x_{\text{lu}} = \max\left(0, X^i_{\text{tr}} - \overline{X^i_{\text{tr}}}\right)_{\text{upper}}$$

$$\Delta x_{\text{ll}} = \max\left(0, X^i_{\text{tr}} - \overline{X^i_{\text{tr}}}\right)_{\text{lower}}$$

$$\Delta x_{\text{su}} = \max\left(0, X^i_{\text{sep}} - \overline{X^i_{\text{sep}}}\right)_{\text{upper}}$$

$$\Delta x_{\text{sl}} = \max\left(0, X^i_{\text{sep}} - \overline{X^i_{\text{sep}}}\right)_{\text{lower}}$$

**Table 1 CIRA problem definition**

| Parameters | Values |
|---|---|
| *Design variables* | |
| Wing twist | $-3°$ to $+3°$ |
| Wing section shape | $-0.25$ to $+0.25$[a] |
| *Design point* | |
| $M_\infty$ | 1.6 |
| $Re_\infty$ | $51.8 \times 10^6$ |
| Reference chord | 6.27 m |
| Altitude | 44,000 ft |
| Lift coefficient | $C_L = 0.182$ |
| *Constraints* | |
| Lift coefficient | $\tilde{C}_L = 0.180$ |
| Pitching moment | $\tilde{C}_M = -0.05$ |
| Trailing-edge angle | $\tilde{\text{tea}} = 0.050$ rad |
| Leading-edge radius | $\tilde{\text{ler}} = 0.002$ m |
| Laminar extent us[b] IW[c] | $X_{\text{tr}} = 0.35$ |
| Laminar extent LS IW | $X_{\text{tr}} = 0.35$ |
| Laminar extent US OW | $X_{\text{tr}} = 0.45$ |
| Laminar extent LS OW | $X_{\text{tr}} = 0.35$ |
| laminar separation | $X_{\text{sep}} = 0.60$ |
| Drag coefficient[d] | $\tilde{C}_D = 0.0195$ |
| *Objective* | |
| $\mathbf{G}(C_D, C_L, C_M, \text{ler}, \text{tea}, \delta x_{\text{lam}})$ | To be minimized |

[a]This is the range of variation of the weights $w_i$ that multiply the shape-modification functions, as mentioned in Sec. VII.A.1.
[b]US stands for upper side; LS stands for lower side.
[c]IW stands for inboard wing; OW stands for outboard wing
[d]Vortex and wave drag.

Here, $\overline{X^i_{\text{tr}}}$ and $\overline{X^i_{\text{sep}}}$ are the computed values of transition and separation point at span section $i$, $X^i_{\text{tr}}$ and $X^i_{\text{sep}}$ are the desired values of transition and separation point at span section $i$, and $n$ is the number of streamwise stations defined along the wingspan. Separation point is the chordwise abscissa at which the laminar boundary-layer calculation stops for each section: this can occur either because of a laminar separation (e.g., caused by a separation bubble) or because the boundary-layer solution does not converge at that point for some reason. Separation is taken into account in the $\Delta x_{\text{lam}}$ objective function, because when it occurs upstream of the transition location, transition is automatically switched, even if the $N$ factor has not yet reached the critical value. This approach is used in order to delay the laminar separation point as much as possible.

The constraint value on inviscid drag and the set of desired transition locations have been assigned following preliminary studies and past experiences in laminar wing design. In particular, the drag penalty is activated with a huge weight when the inviscid drag exceeds the baseline value (195 drag counts). On the other hand, the transition specifications that have been imposed in the design problem represent a sort of utopia point, i.e., the actual threshold above which laminar flow would become really beneficial on aircraft performances and emissions.

### B. Local Approach (ONERA)

*1. Parameterization*

The chosen parameterization is based on 14 design variables, among which one is the angle of attack, five are the twist angles in five control sections chosen along the span, four are the relative leading-edge camber deformation extents, and the remaining four correspond to the maximum deformation amplitudes (Fig. 6, right). The parameterization of the leading-edge camber is the result of a preliminary study that has shown that the $C_p$ peak is very sensitive to such leading-edge region modification. The drop in the $C_p$ peak amplitude is significant, and so is the following recompression. Even though the outboard NLF extent is considered, the whole wing design is parameterized in order to maximize this extent.

*2. Optimization Problem*

In the local approach, the drag reduction is not an active constraint, but a filtering constraint. This means that the final population generated by the optimizer that satisfies the constraints is filtered in order to satisfy the filtering constraints. The objective function is

**Table 2 ONERA problem definition**

| Parameters | Values |
|---|---|
| *Design variables* | |
| Wing twist (five control sections) $nu_i$ | $-3°$ to $+3°$ |
| LE[a] deformation extent (four control sections) $x_i$ | 20% to 50% of local chord |
| LE deformation amplitude (four control sections) $\delta z_i$ | 0 to 0.1 m |
| Angle of attack $\alpha$ | 0 to 5° |
| *Design point* | |
| $M_\infty$ | 1.6 |
| $Re_\infty$ | $51.8 \times 10^6$ |
| Reference chord | 6.27 m |
| Altitude | 44,000 ft |
| Lift coefficient | $C_L = 0.182$ |
| *Constraints* | |
| Lift coefficient | $\tilde{C}_L \ge 0.180$ |
| Pitching moment | $\tilde{C}_M = -0.02$ |
| *Filtering constraints* | |
| Nonviscous drag coefficient[b] | $\tilde{C}_D \le C_D$ (baseline, $C_L = 0.182$) |
| Trailing-edge angle (always satisfied) | $\tilde{\text{tea}} = 0.050$ rad |
| Leading-edge radius | $\tilde{\text{ler}} = 0.002$ m |
| *Objective* | |
| **G**: laminar extent on upper outboard | To be maximized |

[a]Leading edge.
[b]Vortex and wave drag.

directly expressed as a laminar-extent surface ratio. The optimization problem formulation is summarized in Table 2.

## VIII. Results

### A. Baseline Wing–Body Analysis

Before getting into the design process, the reference configuration has been analyzed in order to have a comparison to quantify the achievable performance gain during the optimization task. Moreover, a preliminary mesh tuning and sensitivity analysis has been carried out in order to find the best parameters and size to get a good compromise between the level of accuracy and the computational speed. Both structured meshes are made of nearly $10^6$ nodes and are depicted in Figs. 7. The flow conditions are shown in Table 3.

The aerodynamic analysis of the baseline reference configuration showed that a very limited amount of laminar flow can be achieved on such a configuration. Figure 8 shows the pressure coefficient curves at the wingspan stations reported in the same figure. A strong expansion region is observed around the kink section, and the discontinuity in the leading-edge sweep angle gives rise to an oblique shock wave that propagates toward the wing tip with an angle equal to the inboard-wing sweep (65°). At the same time, the presence of an expansion peak on the suction side downstream of the attachment line is evident throughout all the wing stations, and its intensity is very important in the inboard region. This phenomenon, together with the oblique shock wave, completely inhibits the possibility to find a long run of laminar flow on the wing surface. Indeed, the laminar boundary-layer computation stops quite early, due to laminar separation problems, except near the reference station (at $y = 5612$ mm), because the wing airfoil was designed to match the conditions in this section. Furthermore, the $N$ factor is already very high in the computed region, triggering the transition very early along the whole wingspan. The $N$-factor distributions, with a cutoff at $N = N_{\text{crit}}$, on the upper and lower sides of the baseline wing are presented in Fig. 9.

As can be seen in Fig. 9, the laminar region ($N < N_{\text{crit}}$) is mainly confined near the leading edge. The NLF extent in this region represents less than 4% of chord length of the outboard upper surface. The laminar extent is detected using a critical $N$ factor of 10. This value is very conservative, as it is typically used for 2-D transonic configurations. As mentioned in Sec. VI.E, a more realistic value of the $N$ factor for a 3-D transonic configuration would typically be around 15. On the other hand, the slope of the computed $N$-factor curves on the baseline shape (and hence the spatial growth of boundary-layer disturbances) is so steep that even a variation on the choice of the critical $N$ factor would not bring significant differences in transition prediction. For the above-described reasons, the reference configuration represents a critical starting point for the design optimization, and strong airfoil shape modifications are expected near the wing leading edge in order to prevent unfavorable aerodynamic features.

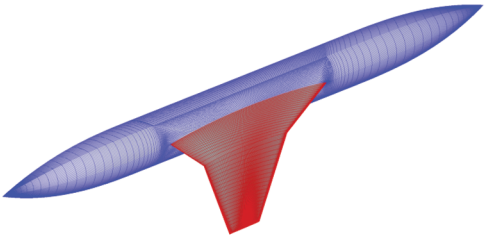

a) Global approach

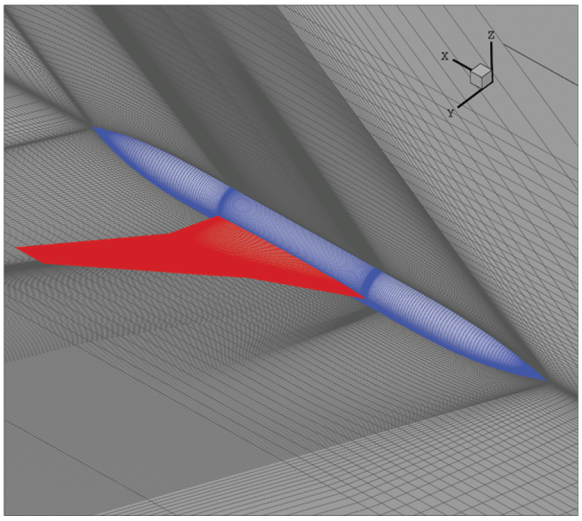


b) Local approach

**Fig. 7 Sketch of structured meshes.**

**Table 3 Flow conditions**

| Parameters | Values |
|---|---|
| Mach | 1.6 |
| Reynolds | $51.8 \times 10^6$ |
| $L_{\text{ref}}$, m | 6.27 |
| Wing area, m$^2$ | 50 |
| AOA, ° | 3.65 |
| $C_L$ | 0.183 |

### B. Optimization Behavior

*1. Global Optimization*

The optimized wing–body configuration is the result of a complex and articulated design process. It has involved several genetic

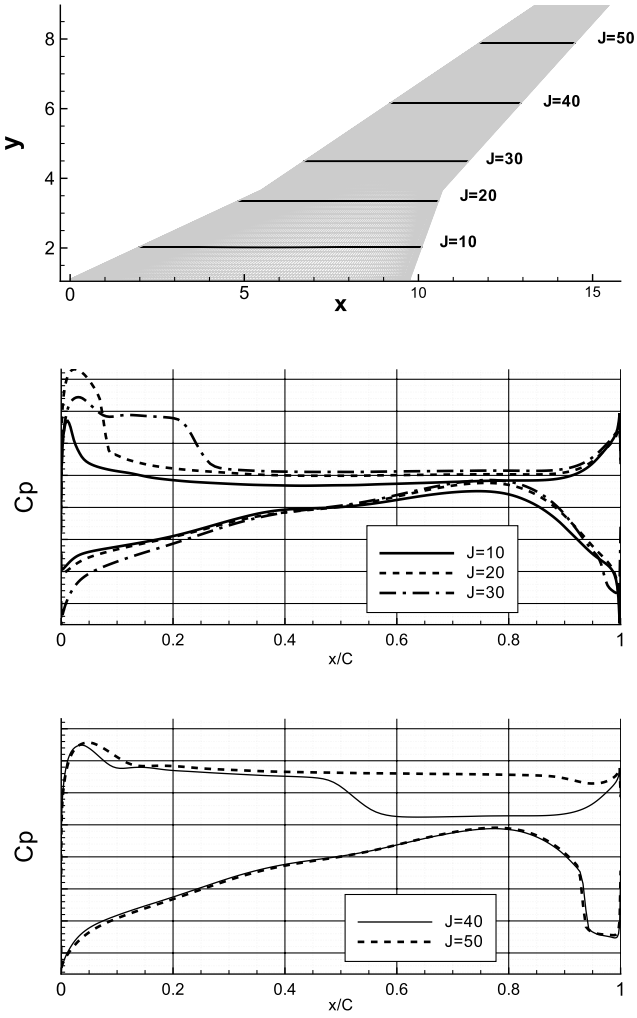


**Fig. 8 Baseline pressure distribution at selected spanwise stations.**

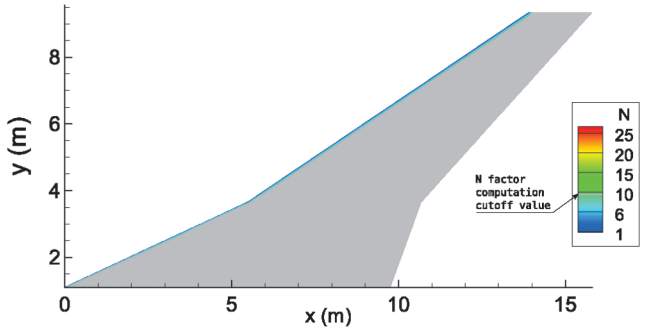


a) Upper side

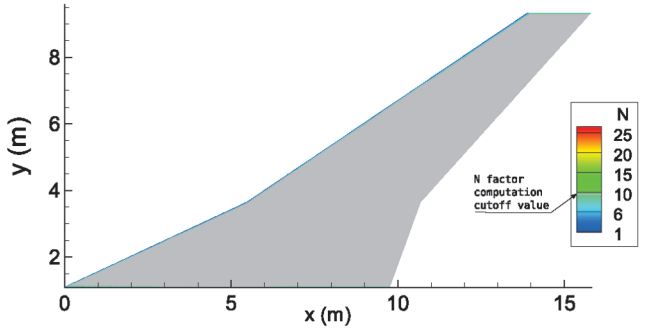


b) Lower side

**Fig. 9 *N*-factor maps on baseline wing.**

optimization cycles, both single objective and multiobjective, each with different settings and strategies. A first optimization stage has been performed considering the wing alone (without the fuselage) in order to investigate the effect of shape and twist modification on supersonic laminar flow in a simpler and rather ideal case. Indeed, it was expected that a homogeneous incoming flow in terms of Mach and Reynolds numbers would have enhanced the possibility to get an extensively laminar boundary layer on the wing surface. The performance-degradation effect of the fuselage was considered in the final design step. Here, the starting point was the already-optimized isolated wing coupled to the Dassault Aviation fuselage. The convergence history of this last genetic algorithm run is depicted in Fig. 10; it can be observed that the ratio between the initial value of the objective function and the final one is about 4. This figure shows a further strong improvement in the fitness, even in the presence of the fuselage. In fact, the optimal design (wing and fuselage) achieves the same level of performance as the initial configuration of the last run (optimized isolated wing), which was designed without taking into account the fuselage effect. This last result has been obtained by changing only the wing shape, and hence it shows how proper shape modifications can be effective to balance the laminar performance loss due to the fuselage.

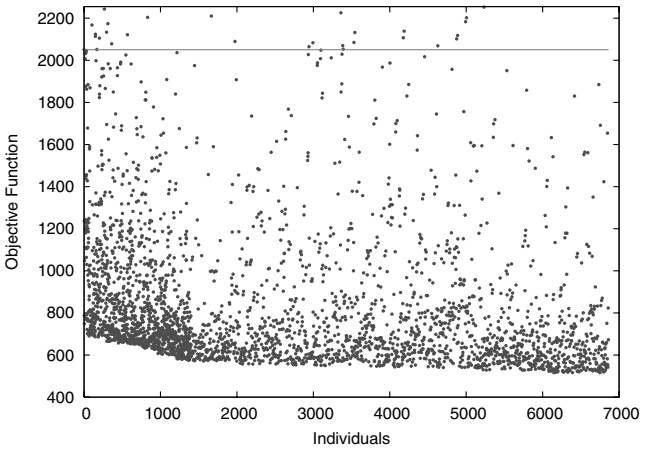


**Fig. 10 GAW final run convergence history.**

*2. Local Optimization*

A family of enhanced shapes was found after nearly 500 evaluations (Figs. 11 and 12), with each evaluation implying flow and transition analysis that required up to 20 min on a NEC SX8 supercomputer. The final optimal shape was then obtained by filtering the design that underwent the minimum deformation extent in terms of twist (the most relevant parameter in this case), compared with the reference case, with a maximum laminar extent. As mentioned previously, even though the drag was not taken into consideration during the optimization process, it has been checked that the inviscid pressure drag variation, compared with the baseline, was negligible.

The optimizer reached 7.1% of laminar surface instead of 4.7% for the initial shape for a critical $N$ factor set to 10. The laminar extent corresponding to a higher value of this $N$ factor would, of course, be more important. For instance, for $N_{\text{crit}} = 15$ the laminar extent is multiplied by 2. Both lift and pitching moment constraints are satisfied.

### C. Enhanced Configurations Analysis

*1. Global Optimization*

The impact of the optimization process on wing pressure distribution is shown in Fig. 13; the contour lines and the $C_p$ curves highlight the continuity and the low level of flow expansion on the suction side. As a consequence, the recompression phenomena are present only around the trailing edge and in the wake region where

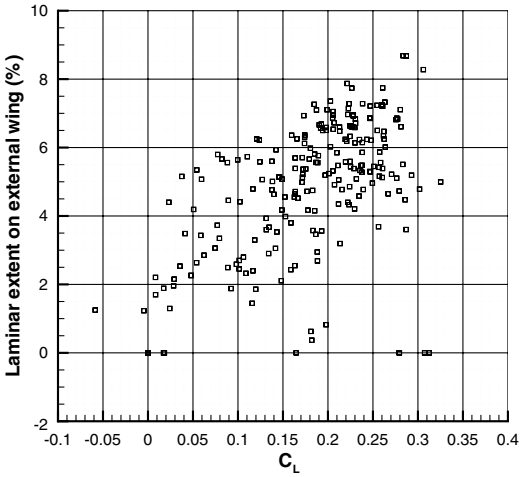


**Fig. 11 $C_L$ vs laminar extent.**

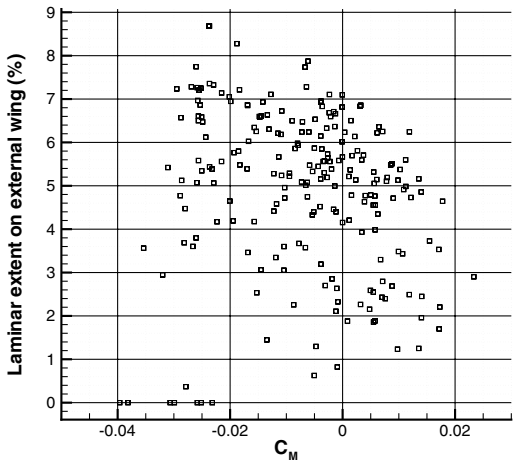


**Fig. 12 $C_M$ vs laminar extent.**

the contact between the upper and lower flows occurs. The comparison with the pressure solution on the baseline gives evidence of a completely new redesign of the whole wing upper side.

Surface pressure distribution strongly influences the mechanisms, which leads to laminar-to-turbulent transition onto a wing. In fact, a careful design of the pressure gradient can delay the amplification of boundary-layer disturbances and passively control attachment line, crossflow, and Tollmien–Schlichting instabilities. In the present case, the evolutionary optimization algorithm has been used to naturally enhance the pressure coefficient characteristics by shape design toward the maximization of natural laminar flow in real supersonic flight conditions. Past studies [56] and present optimization results show that two most important design features can be identified: the chordwise pressure gradient near the attachment line and aft the leading edge. Only the combined optimization of both can result in an effective performance improvement. Indeed, the attachment-line Reynolds number ($\bar{R} = W_e/\sqrt{\nu \tilde{U}_e}$) is directly proportional to the spanwise velocity component $W_e$ and inversely proportional to the chordwise velocity gradient $\tilde{U}_e$ evaluated on the attachment line. Obviously, the latter depends on the shape of the airfoil around the leading edge and, in particular, on the leading-edge radius. Hence, through the design of a strong acceleration profile with small leading-edge radius, it is possible to prevent the attachment-line instability. However, a tradeoff must be found with the imposed constraint on minimum leading-edge radius value and with the need for avoiding strong leading-edge pressure peaks, which would feed the streamwise disturbances. Such a tradeoff has been found in the present research and highlighted in Fig. 14, where the attachment-line velocity component $W_e$, the chordwise velocity gradient $\tilde{U}_e$, and the resulting $\bar{R}$ are plotted against the wingspanwise coordinate. Both the compressible and incompressible formulation of $\bar{R}$ are reported, showing negligible differences. The value of $\bar{R}$ at each wing section has been drawn from the CFD solution. The CFD Cartesian velocity components are transformed by the boundary-layer code and its local reference system into the local spanwise and chordwise velocity components; hence, it is straightforward to draw $W_e$ and $\tilde{U}_e$. The latter is obtained through a simple derivation operation, which provides more accurate results with a smaller spatial step size $\Delta x/c$.

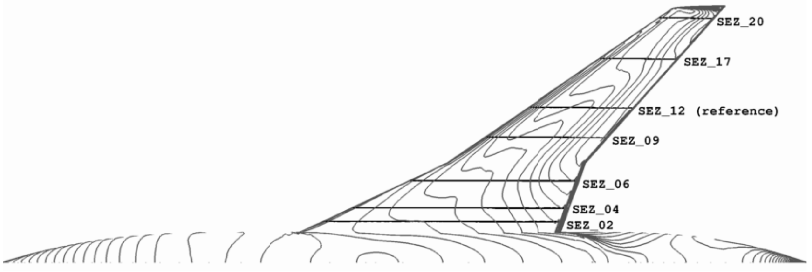


**a) Cut sections along span on $C_p$ contour lines**

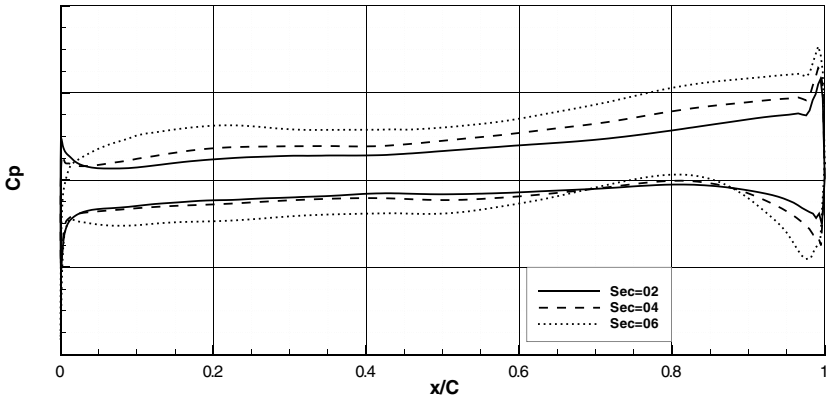


**b) Sectional pressure coefficient, inner wing**

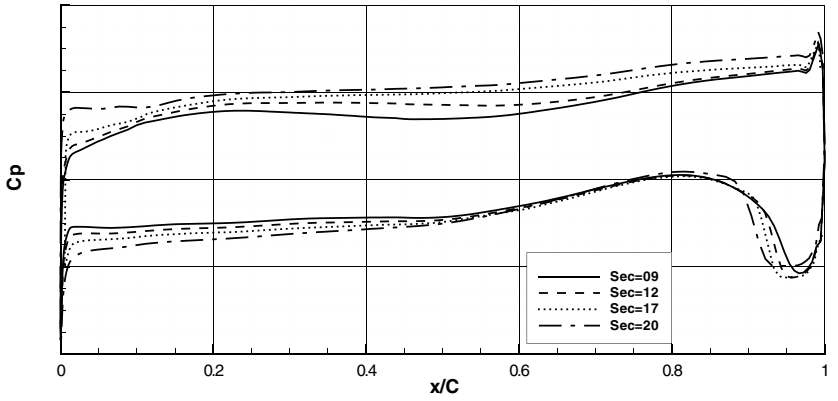


**c) Sectional pressure coefficient, outer wing**

**Fig. 13 Global optimum aerodynamic solution.**

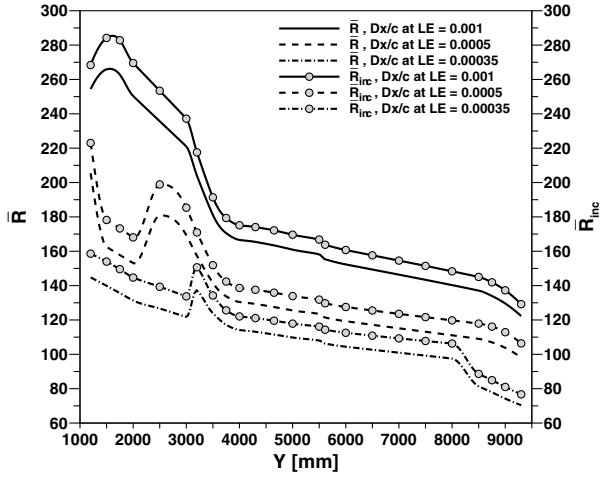


**a) Compressible and incompressible $\bar{R}$**

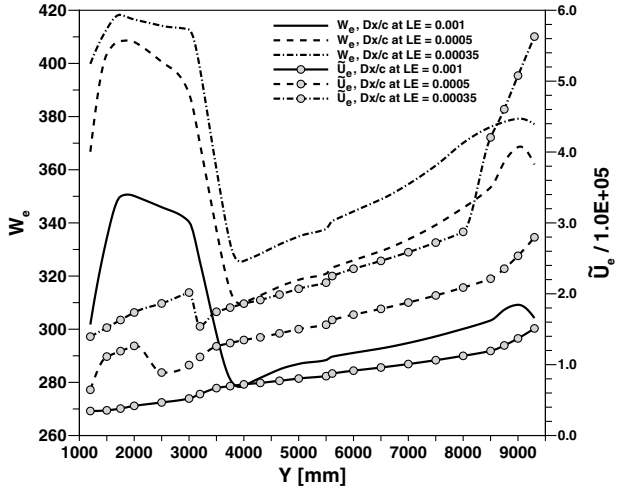


**b) $W_e$ velocity component and $\tilde{U}_e$ velocity gradient**

**Fig. 14 Global optimum, Poll criterion parameters computation for attachment-line contamination vs spanwise axis.**

$W_e$ and $\tilde{U}_e$ have been computed at various chordwise abscissa steps ($\Delta x/c$) near the attachment-line location. In Figs. 14a and 14b, the curves obtained for three values of $\Delta x/c$ (0.001, 0.0005, and 0.00035) are reported: $\bar{R}$ falls well below Poll's threshold of 245 as the accuracy of the calculation increases. The chordwise velocity gradient in Fig. 14b shows the effect of the proper shape design carried out by the evolutionary algorithm; the gradient levels are very high at each wing section and the trend to increase along the span direction balances the growth of the spanwise velocity due to the high-sweep angle effect, thus causing the observed decrease of $\bar{R}$. Just a little farther downstream, pressure rapidly falls in order to minimize the chordwise extent of maximum crossflow growth in the leading-edge region. A slight peak can appear at the end of this limited region to minimize the crossflow growth, as discussed in [57]. Thereafter, the pressure gradient is very small and favorable (negative pressure gradient), to damp the Tollmien–Schlichting wave amplification. Here, another tradeoff has been found, as this continuous pressure decrease must not be strong enough to cause excessive shock losses farther downstream and even flow separation at the design point. The pressure drag constraint was added just to control this feature and effectively acted to avoid big drag rises at the design point.

Another issue toward NLF enhancement is related to the wing planform. The double-leading-edge sweep angle and the strong taper-ratio distribution contribute to set significantly different aerodynamic conditions at each wing section. Indeed, not only is the crossflow pattern very sensitive to sweep angle change and taper ratio, which alter the spanwise pressure gradient, but the Reynolds number also varies from about $75 \times 10^6$ at the root section to $16 \times 10^6$ at the tip. Hence, as a result of the attempt to passively control the NLF amplification mechanisms under modified external conditions through shape optimization, the wing surface is shaped from sections having completely different geometric characteristics. An example is the tendency to nose-droop that is not observed in the inner sections, but is present in the kink midwing region: here, indeed, an interesting and not-expected tradeoff solution has been found by the optimizer. On one hand, the optimizer reduced the leading-edge radius as much as possible to avoid crossflow and attachment-line contamination in a critical zone where a discontinuity in attachment-line flow has been detected; on the other hand, moderate pressure peaks arose and the optimizer tried to damp them through nose-drooping. More details about the optimized wing airfoil's shape can be found in SUPERTRAC project technical reports [28,58].

The main result of global search optimization is the general observable decrease of $N$-factor levels along the whole wing. This is a key feature because, even if the choice of the critical value of $N$ (and hence of the transition location) can be discussed, the advantages of having lower disturbance growth rates are clear and make the application of additional (active) boundary-layer flow control techniques much more effective. The envelope curves as computed by the database method for several wing stations are reported in Figs. 15–18. Both on the upper and lower wing surfaces, transition is triggered mainly by combined TS-CF wave amplification, except near the wing-fuselage intersection, where the leading-edge shape dulls the CF waves. Adopting 15 as the critical $N$ factor, the transition lines onto the optimal wing surface are extracted and plotted in Fig. 19 as the chord percentage of laminar flow extent along the wingspan. As expected, the transition location is placed more downstream for airfoil sections located near the wing tip, due to the Reynolds number decreasing effect. The surface of laminar flow has been increased from 4.7 to 21% on the suction side and from 10 to 33% on the pressure side.

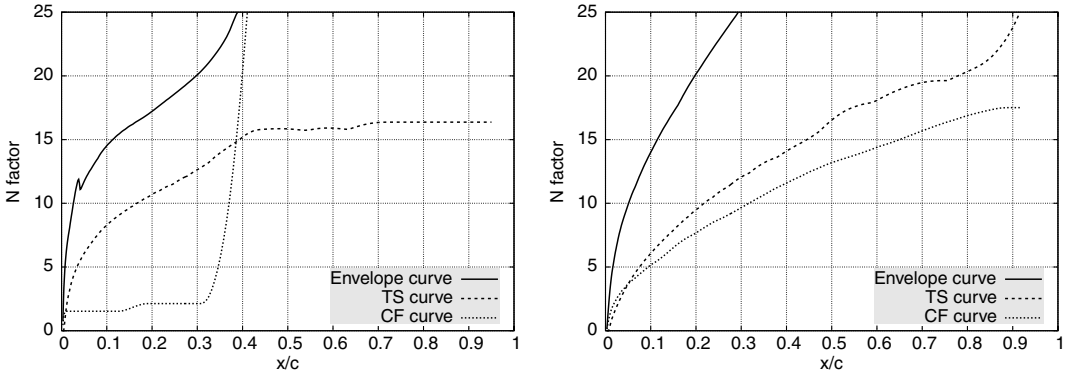


**Fig. 15 Stability curves for optimal wing section shape SEZ02: upper (left) and lower (right) sides.**

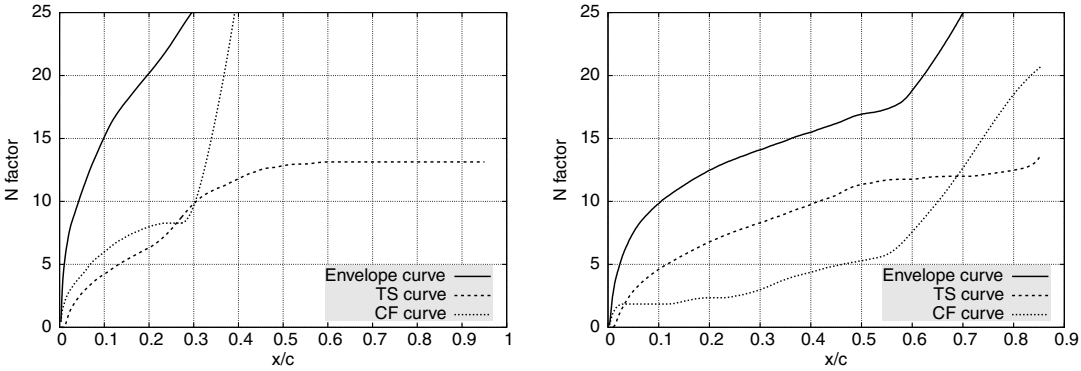


**Fig. 16 Stability curves for optimal wing section shape SEZ06: upper (left) and lower (right) sides.**

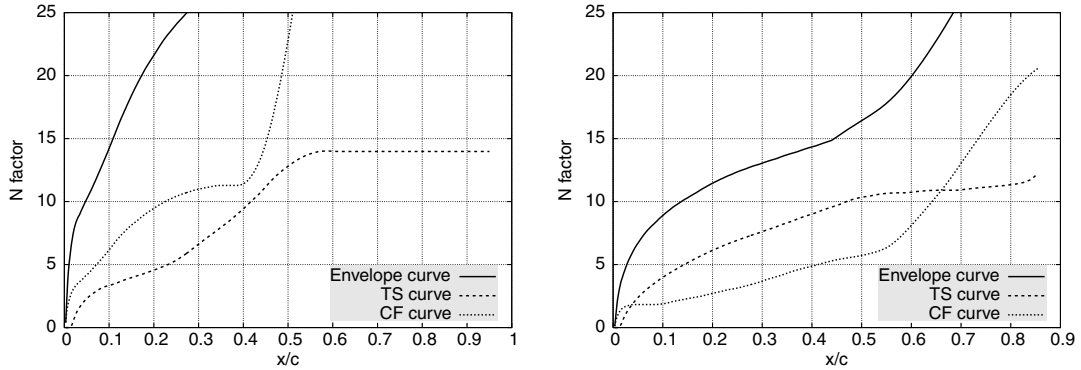


**Fig. 17 Stability curves for optimal wing section shape SEZ12: upper (left) and lower (right) sides.**

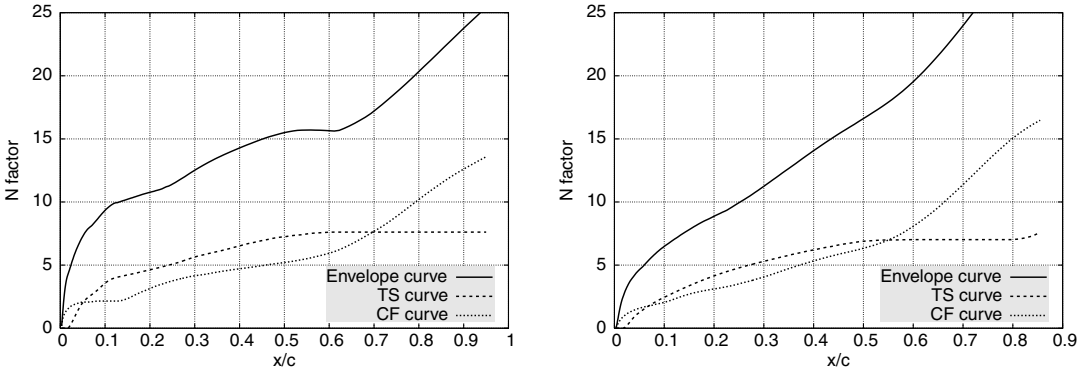


**Fig. 18 Stability curves for optimal wing section shape SEZ20: upper (left) and lower (right) sides.**

Figure 20 shows the *N*-factor evolution map on the upper wing surface for the global optimum wing, as computed by ONERA using the 3C3D code and the database method; results are very close to CIRA predictions.

### 2. *Local Optimization*

The impact of the optimization process on the $C_p$ distribution (Fig. 21) is very instructive. The $C_p$ peak on the upper side has been very consequently reduced. The distribution has even been flattened for the inner wing section, and is very similar to the 2-D distribution. The counterpart of this flattening at the leading edge is a progressive expansion until 30%, with strong spanwise variation in the slope. It can also be observed that the shocks have been smoothed on the upper side. On the lower side, note stronger shocks at the trailing-edge level and hence increasing the drag penalty.

Regarding the performance in terms of laminar extent, the resulting optimal shape performance gain, as can be seen on the *N*-factor distribution on the upper side (Fig. 22), is not as important, as expected. A narrow low-*N*-factor area around the kink (blue region) that extends throughout the whole wing chord can be noted; here, the boundary-layer stability computation failed due to a flow separation induced by the pressure peak that can be observed in Fig. 21. To check the validity of the laminar-extent evaluation for such a configuration, exact linear stability computations have been performed at two sections, $y = 2.25$ and 6.57 m. The comparison between exact and simplified calculations demonstrates that the database method provides a good estimation of the *N* factor (Fig. 23).

The streamwise coordinates used are the curvilinear abscissa measured from the attachment line; however, the difference between $s$ and $x$ still remains small. Extra configurations have also been studied to understand how a modification of the parameterization could enhance the research of an optimal configuration. The conclusions that have been drawn are that a splinelike twist law instead of linear-by-part law would induce additional drag penalty, but would also increase the laminar flow robustness to the flow

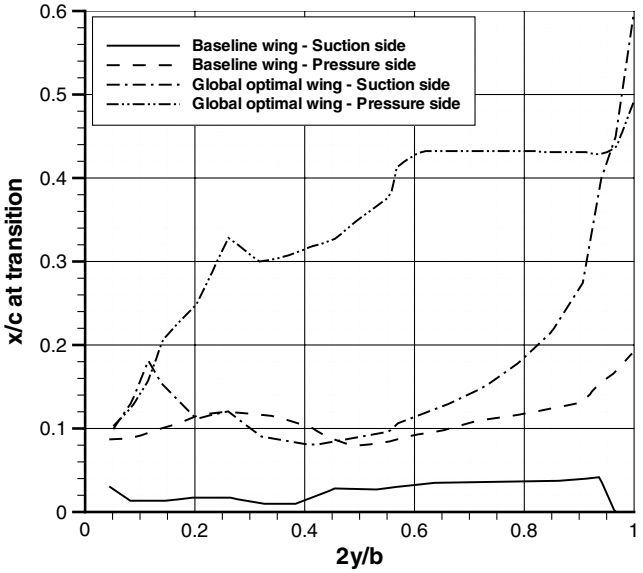


Fig. 19 Transition lines: database method, $N$ factor at transition = 15.

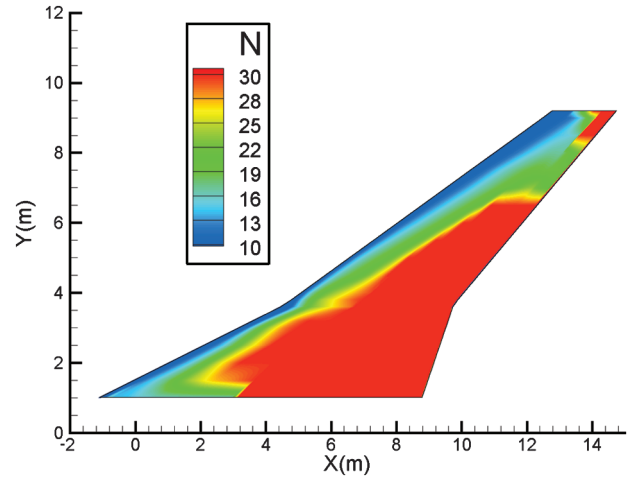


Fig. 20 Global optimization: $N$-factor contour map.

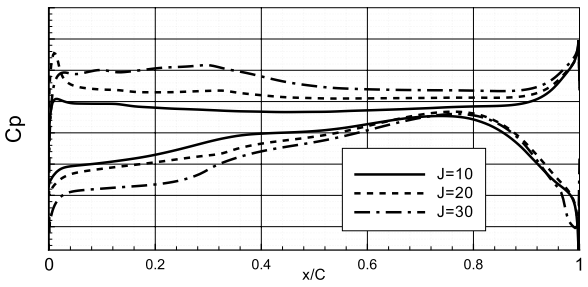


a) Pressure distribution, inner wing

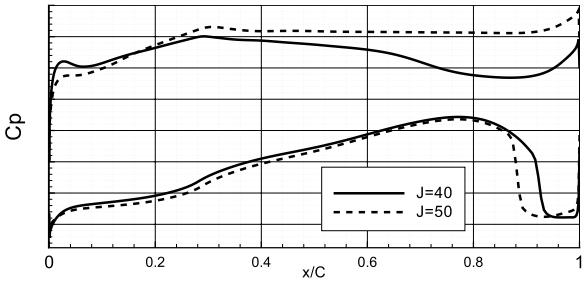


b) Pressure distribution, outer wing

Fig. 21 Local-approach enhanced pressure distribution in five span locations.

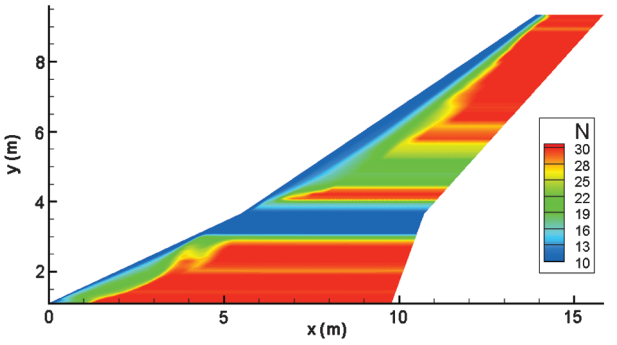


Fig. 22 Local optimization: $N$-factor distribution of optimum.

condition variations. The sweep angle, which was not considered in both optimizations, is also a parameter that has to be taken into account in future design processes.

## IX. Cross-Comparison

In both local and global optimization approaches, it is a fact that the wing laminar extent remains limited in the perspective of an

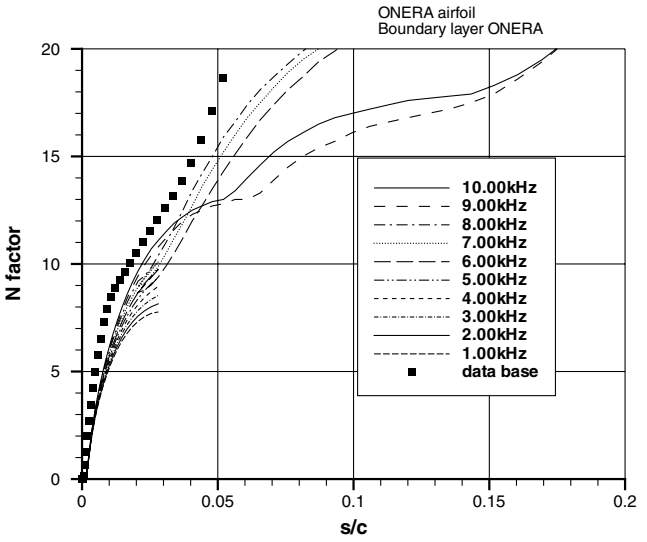


a) Section y=2.25m

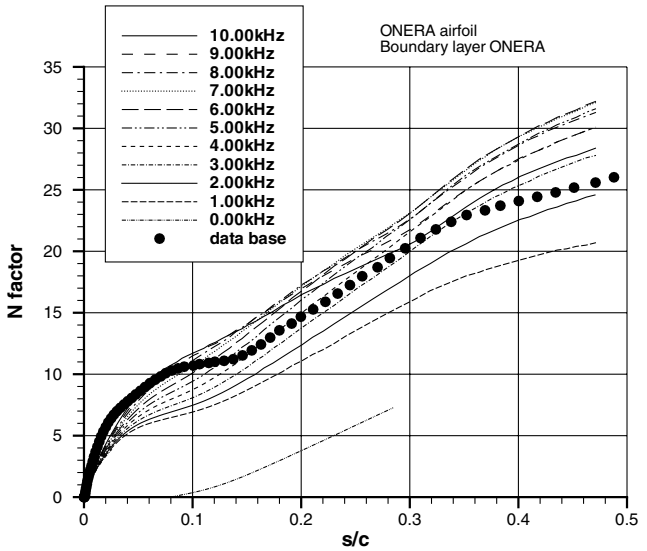


b) Section y=6.57m

Fig. 23 Local optimization: $N$-factor distributions.

appreciable friction-drag reduction. On the upper side, the global-approach wing gives better results on the inboard and the outboard near the tip, whereas the local-approach wing provides better results on the outboard center part. On the lower side, neither the global nor the local approach designs show a significant laminar extent on the inboard wing, whereas the global approach performs better on the outboard region. The inboard has a very limited laminar extent in both cases. However, global-approach $N$-factor levels are lower, which is more convenient for a hybrid transition control application. As a matter of fact, a detailed study of both wings performance at different flight points with and without suction has been achieved within the same project [59] and has shown that wings designed toward NLF enhancement are more suitable than nonoptimized configurations for active flow control.

## X. Conclusions

The objective of the presented study was to verify the possibility to perform shape optimization for natural laminar flow maximization in the supersonic regime. One important result is that for such a configuration (high Mach number, high-sweep angle, and low aspect ratio) the three-dimensional effects are dominant and strongly affect the inviscid pressure distributions and the boundary-layer velocity profiles. Hence, having a full set of 3-D tools during the optimization process is mandatory.

The chosen strategies and computational tools have proved to be sufficiently robust to successfully perform both optimizations. Indeed, the use of fast stability analysis using analytical approximations and database techniques was very efficient and robust, considering the three-dimensional complexity of the problem. The comparison of both wings using a single method (envelope $N$ factor) and common tools has shown that achieving substantial NLF-extent improvement with shape optimization remains a challenge for such configurations. However, both 3-D optimizations have led to enhanced configurations that show superior performances with respect to the reference in terms of hybrid laminar flow control.

From the design-solution point of view, the common conclusion of the presented optimizations is that sensitivity to NLF of such a configuration is clearly driven (for a given planform, twist angle, and thickness law) by the leading-edge parameters such as the leading-edge radius and camber. Future investigations should look in the direction of a deeper knowledge of the correlations between these and other parameters that have not been varied in the present study, e.g., the sweep angle, and their combined effects on supersonic laminar flow control.

## References


[1] Smith, A. M. O., and Gamberoni, N., "Transition, Pressure Gradient and Stability Theory," Douglas Aircraft Co., Rept. ES 26388, Long Beach, CA, 1956.

[2] Arnal, D., "Boundary Layer Transition: Predictions Based on Linear Theory," AGARD, TR 793, 1994.

[3] Yoshida, K., and Makino, Y., "Aerodynamic Design of Unmanned and Scaled Supersonic Experimental Airplane in Japan," *ECCOMAS Congress*, 2004.

[4] McTigue, J. G., Overton, J., and Petty, G. J., "Two Techniques for Detecting Boundary-Layer Transition in Flight at Supersonic Speeds and at Altitudes Above 20,000 Feet," NASA, TN D-18, 1959.

[5] Banks, D. W., van Dam, C. P., Shiu, H. J., and Miller, G. M., "Visualization of In-Flight Flow Phenomena Using Infrared Thermography," *9th International Symposium on Flow Visualization*, 2000.

[6] Saric, W. S., Reed, H. L., and Banks, D. W., "Flight Testing of Laminar Flow Control in High-Speed Boundary Layers," *Enhancement of NATO Military Flight Vehicle Performance by Management of Interacting Boundary Layer Transition and Separation*, Research and Technology Organization, Neuilly-sur-Seine, France, 2004.

[7] Sturdza, P., "An Aerodynamic Design Method for Supersonic Natural Laminar Flow Aircraft," Ph.D. Thesis, Stanford Univ., Stanford, CA, 2003.

[8] Kroo, I., "Unconventional Configurations for Efficient Supersonic Flight," *Innovative Configurations and Advanced Concepts for Future Civil Aircraft*, VKI Lecture Series, von Karman Inst. of Fluid Dynamics, Rhode-Saint-Genèse, Belgium, 2005, pp. 1–25.

[9] Tokugawa, N., Kwak, D.-Y., Yoshida, K., and Ueda, Y., "Transition Measurement of Natural Laminar Flow Wing on Supersonic Experimental Airplane NEXST-1," *Journal of Aircraft*, Vol. 45, 2008, pp. 1495–1504. doi:10.2514/1.33596

[10] Ishikawa, H., Kwak, D.-Y., and Yoshida, K., "Numerical Analysis on Flight-Test Results of Supersonic Experimental Airplane NEXST-1," *Journal of Aircraft*, Vol. 45, 2008, pp. 1505–1513. doi:10.2514/1.33595

[11] Fujita, T., Matsushima, K., and Nakahashi, K., "Aerodynamic Wing Design of NEXST-2 Using Unstructured-Mesh and Supersonic Inverse Problem," *Journal of Aircraft*, Vol. 41, 2004, pp. 1146–1152. doi:10.2514/1.3455

[12] *First European Forum on Laminar Flow Technology*, Deutsche Gesellschaft fuer Luft- und Raumfahrt, Hamburg, Germany, March 1992.

[13] Wagner, R., Maddalon, D., Bartlett, D., and Collier, F., "Fifty Years of Laminar Flight Testing," Society of Automotive Engineers, TR 881393, Warrendale, PA, 1988.

[14] Horstmann, K. H., and Miley, S. J., "Comparison of Flight and Wind Tunnel Investigations of Tollmien–Schlichting Waves on an Aircraft Wing," *First European Forum on Laminar Flow Technology*, March 1992, pp. 45–51.

[15] Horstmann, K. H., Quast, A., and Redeker, G., "Flight and Wind-Tunnel Investigation on Boundary-Layer Transition," *Journal of Aircraft*, Vol. 27, No. 2, 1990, pp. 146–150. doi:10.2514/3.45910

[16] Schrauf, G., Perraud, J., Vitiello, D., Stock, H. W., Abbas, A., and Lam, F., "Transition Prediction with Linear Stability Theory—Lessons Learned from the ELFIN F100 Flight Demonstrator," *2nd European Forum on Laminar Flow Technology*, Bordeaux, France, June 1996.

[17] Arnal, D., Casalis, G., and Schrauf, G., "The EUROTRANS Project (EUROpean TRANSition)," *2nd European Forum on Laminar Flow Technology*, Association Aéronautique et Astronautique de France, Bordeaux, France, June 1996.

[18] Schrauf, G., Bieler, H., and Thiede, P., "Transition Prediction—The Deutsche Airbus View," *First European Forum on Laminar Flow Technology*, Deutsche Gesellschaft fuer Luft- und Raumfahrt, Hamburg, Germany, March 1992.

[19] Pfenninger, W., "Laminar Flow Control-Laminarization," AGARD, TR 654, Neuilly-sur-Seine, France, June 1977.

[20] Poll, D. I. A., "Transition in the Infinite Swept Attachment Line Boundary Layer," *Aeronautical Quarterly*, Vol. 30, 1979, pp. 607–628.

[21] Poll, D. I. A., "Some Aspects of the Flow Near a Swept Attachment Line with Particular Reference to Boundary Layer Transition," College of Aeronautics, Cranfield Univ., TR 7805/K, Cranfield, England, U.K., 1978.

[22] Poll, D. I. A., "Boundary Layer Transition on the Windward Face of Space Shuttle During Reentry," AIAA Paper 1985-0899, 1985.

[23] Morkovin, M., "Instability, Transition to Turbulence and Predictability," AGARD, TR 236, Neuilly-sur-Seine, France, July 1978.

[24] Morkovin, M., "Recent Insights into Instability and Transition to Turbulence in Open-Flow Systems," NASA Langley Research Center, CR 181693, Hampton, VA, 1988.

[25] Mack, L. M., "Boundary Layer Linear Stability Theory," Special Course on Stability and Transition of Laminar Flows, AGARD, 709, Neuilly-sur-Seine, France, 1984.

[26] Mack, L. M., "On the Stability of the Boundary Layer on a Transonic Swept Wing," AIAA Paper 79-0264, 1979.

[27] Van Ingen, J., "A Suggested Semi-Empirical Method for the Calculation of the Boundary Layer Transition Region," Delft Univ. of Technology, Department of Aerospace Engineering, TR VTH-74, Delft, The Netherlands, 1956.

[28] Iuliano, E., Quagliarella, D., and Donelli, R., "Design of a Supersonic High-Swept Wing NLF Airfoil: SUPERTRAC Sub-Task 4.1.5," Italian Aerospace Research Center, TR SPT-CIRA-41-002, Capua, Italy, 2006.

[29] Jameson, A., "Aerodynamic Design Via Control Theory," NASA Langley Research Center, TR 88-64, Hampton, VA, 1988.

[30] Vitagliano, P. L., and Quagliarella, D., "A Hybrid Genetic Algorithm for Constrained Design of Wing and Wing–Body Configurations," *Evolutionary Methods for Design, Optimization and Control Applications to Industrial and Societal Problems*, edited by G. Bugeda, J. A. Désidéri, J. Périaux, M. Schoenauer, and G. Winter, International Center for Numerical Methods in Engineering, Barcelona, 2003.

[31] Quagliarella, D., and Vicini, A., "Gas for Aerodynamic Shape Design II: Multiobjective Optimization and Multicriteria Design," *Lecture Series 2000-07, Genetic Algorithms for Optimisation in Aeronautics*

*and Turbomachinery*, von Karman Inst. of Fluid Dynamics, Rhode-Saint-Genèse, Belgium, May 2000.

[32] Quagliarella, D., and Vicini, A., "Gas for Aerodynamic Shape Design I: General Issues, Shape Parametrization Problems and Hybridization Techniques," *Lecture Series 2000-07, Genetic Algorithms for Optimisation in Aeronautics and Turbomachinery*, von Karman Inst. of Fluid Dynamics, Rhode-Saint-Genèse, Belgium, May 2000.

[33] Deb, K., *Multi-Objective Optimization Using Evolutionary Algorithms*, Wiley, New York, 2001.

[34] Rasheed, K., "GADO: A Genetic Algorithm for Continuous Design Optimization," Ph.D. Thesis, Rutgers Univ., New Brunswick, NJ, 1998.

[35] Eldred, M. S., Adams, B. M., Gay, D. M., Swiler, L. P., Haskell, K., Bohnhoff, W. J., et al., " Sandia National Labs., TR SAND2006-6337, Albuquerque, NM, Dec. 2008.

[36] Anderson, M. B., and Gebert, G. A., "Multi-Disciplinary Optimisation of a Supersonic Transport Aircraft Wing Planform," *European Congress on Computational Methods in Applied Sciences and Engineering (ECCOMAS 2004)*, July 2004.

[37] Quagliarella, D., Iannelli, P., Vitagliano, P. L., and Chinnici, G., "Aerodynamic Shape Design Using Hybrid Evolutionary Computation and Fitness Approximation," AIAA 1st Intelligent Systems Technical Conference, AIAA Paper 2004-6514, Chicago, Sept. 2004.

[38] Spekreijse, S. P., Boerstoel, J. W., Vitagliano, P. L., and Kuyvenhoven, J. L., "Domain Modeling and Grid Generation for Multiblock Structured Grids with Application to Aerodynamic and Hydrodynamic Configurations," NASA CP-3143, edited by R. E. Smith, 1992, pp. 207–229.

[39] Boerstoel, J. W., Jacobs, J. M. J. W., Kassies, A., Amendola, A., Tognaccini, R., and Vitagliano, P. L., "Applications of Mesh Generation to Complex 3-D Configurations," AGARD CP-464, May 1989, Paper 9.

[40] Boerstoel, J. W., Spekreijse, S. P., and Vitagliano, P. L., "The Design of a System of Codes for Industrial Calculations of Flows Around Aircraft and Other Complex Aerodynamic Configurations," AIAA Paper 1992-2619, 1992.

[41] Amato, M., and Catalano, P., "Non linear $k$-$\varepsilon$ Turbulence Modeling for Industrial Applications," *ICAS 2000 Congress*, Harrogate, England, U.K., 2000.

[42] Kok, J. C., Amato, M., and Boerstoel, I. W., "Mathematical-Physical Modeling for Multiblock NaS/Euler Simulation," Italian Aerospace Research Center, TR CIRADLCEST-TR183, Capua, Italy, 1991.

[43] Amato, M., and Iaccarino, G., "Mathematical Numerical Modelling for a Multiblock RANS Flow Solver," Italian Aerospace Research Center, TR CIRA-TR-95-140, Capua, Italy, Oct. 1995.

[44] Cambier, L., and Gazaix, M., "elsA: An Efficient Object-Oriented Solution to CFD Complexity," 40th AIAA Aerospace Science Meeting and Exhibit, AIAA Paper 2002-108, Reno, NV, Jan. 2002.

[45] Cebeci, T., "A Computer Program for Calculating Three-Dimensional Laminar and Turbulent Boundary Layers and the Onset of Transition on Wings with and Without Suction," Aerospace Engineering Department, California State Univ., TR DILC-EST-TN-407, Long Beach, CA, Dec. 1993.

[46] Houdeville, R., "Three-Dimensional Boundary Layer Calculation by a Characteristic Method," *Fifth Symposium on Numerical and Physical Aspects of Aerodynamic Flows*, Long Beach, CA, Jan. 1992.

[47] Cebeci, T., and Bradshaw, P., *Physical and Computational Aspects of Convective Heat Transfer*, Springer–Verlag, New York, 1988.

[48] Bradshaw, P., Cebeci, T., and Whitelaw, J., *Engineering Calculation Methods for Turbulent Flows*, Academic Press, New York, 1981.

[49] Arnal, D., "Transition Prediction in Transonic Flows," *IUTAM Symposium Transsonicum III*, Springer–Verlag, New YOrk, 1988.

[50] Arnal, D., and Dupé, C., "Database Method," ONERA, Toulouse, France, 1992.

[51] Casalis, G., and Arnal, D., "Database Method—Development and Validation of the Simplified Method for Pure Crossflow Instability at Low-Speed," ELFIN II European project, TR 145, 1996.

[52] Perraud, J., Arnal, D., Casalis, G., Archambaud, J., and Donelli, R. S., "Automatic Transition Prediction using Simplified Methods," AIAA Paper 2009-1144, 2009.

[53] Perraud, J., Arnal, D., Casalis, G., Archambaud, J., and Donelli, R. S., "Automatic Transition Prediction Using Simplified Methods," *AIAA Journal*, Vol. 47, No. 11, 2009, pp. 2676–2684. doi:10.2514/1.42990

[54] Donelli, R. S., and Casalis, G., "Database Approach—Stationary Mode Treatment," CIRA, TR ALTTACIRA-TR-AEP-01-039, Capua, Italy, April 2001.

[55] Lam, F., and White, P., "Calculation of $N$-Factors Using F100 Flight Test Data—Part 1. The Envelope Method," British Aerospace, TR 134, Filton, England, U.K., 1995.

[56] Braslow, A. L., Maddalon, D. V., Bartlett, D. W., Wagner, R. D., and Collier, F. S., *Applied Aspects of Laminar-Flow Technology*, Progress in Astronautics and Aeronautics, AIAA, Washington, D.C., 1990, pp. 47–78.

[57] Pfenninger, W., and Vermuru, C. S., "High Subsonic Speed LFC Transport Airplanes: Boundary Layer Crossflow Stabilization, Wing Analysis and Design," AIAA Paper 88-0275, Jan. 1988.

[58] Salah El Din, I., Iuliano, E., Quagliarella, D., and Donelli, R., "Design of a Supersonic High-Swept Natural Laminar Flow Wing," ONERA, TR SPT-CIRA-41-003, Paris, 2008.

[59] Tran, D., "Report on Definition of the Reference 3D Shape for Combination of Different LFC Devices," Dassault Aviation, TR D4.6, Paris, 2008.